THE JOURNAL OF PHYSICAL CHEMISTRY C
A JOURNAL OF THE AMERICAN CHEMICAL SOCIETY

pubs.acs.org/JPCC

Article

Single-Molecule Measurements Spatially Probe States Involved in Electron Transfer from CdSe/CdS Core/Shell Nanorods

Published as part of The Journal of Physical Chemistry virtual special issue "125 Years of The Journal of Physical Chemistry".

Rachel M. Morin, Garnett W. Bryant, Elena V. Shevchenko, Yuchen Sha, and Matthew Pelton*

Cite This: *J. Phys. Chem. C* 2021, 125, 21246–21253

Read Online

ACCESS | Metrics & More | Article Recommendations

ABSTRACT: Semiconductor nanorods with charge-accepting molecules adsorbed on their surfaces serve as model systems for solar energy conversion. An electron photoexcited from the valence band of the nanorod to a high-energy state in the conduction band will relax and transfer to a state in the molecule, producing a long-lived charge-separated state that facilitates charge extraction and thereby enables photochemical reactions. Characterizing the dynamics of the charge-separation process and the electronic states involved is essential for a microscopic understanding of photocatalysis involving these materials, but this information is obscured in ensemble measurements due to the random placement of molecules on the nanorod surfaces. Here, we show that measurements on individual CdSe/CdS core/shell nanorods functionalized by single methyl viologen molecules provide information about the distribution of electron-transfer rates from confined states in the nanorods to states in the molecules. By comparing this transfer-rate distribution to the predictions of a tight-binding model, we find that charge transfer most likely involves hot electrons in an excited conduction-band state, rather than electrons that have fully thermalized to the conduction-band edge. The ability to extract hot electrons from semiconductor nanocrystals may help enable energy-efficient photocatalysis, and the single-particle charge-transfer method may serve as a widely applicable tool to probe the spatial distribution of electronic states in nanocrystals.

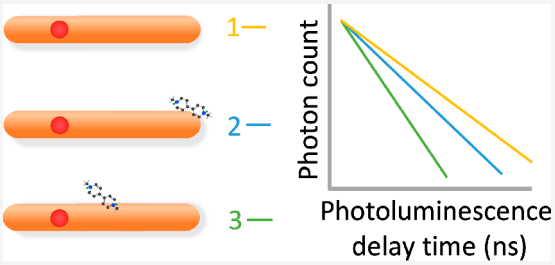

INTRODUCTION

The ability of materials to efficiently absorb light and then transfer excited carriers into long-lived charge-separated states is critical for subsequent use of the separated charges in redox reactions.[1] Hybrid nanomaterials that have been widely investigated for this function typically consist of a semiconductor nanostructure that absorbs photons and a secondary component such as a metal nanostructure, another semiconductor nanostructure, an organic molecule, or an enzyme.[2−4] The secondary structure accepts an electron or hole from an excited state in the semiconductor nanostructure, thereby separating the photogenerated charges and reducing their recombination rate. Optimization of these materials for photocatalysis will benefit from an understanding of the interfacial charge-transfer process, with structures consisting of semiconductor nanocrystals that have charge-accepting molecules on their surfaces providing a particularly convenient and rich model system to study.[5]

The kinetics of charge transfer from nanocrystals to adsorbed molecules is commonly measured by using time-resolved spectroscopy, particularly time-resolved fluorescence decay and transient absorption.[5] However, the different hybrid nanostructures within an ensemble will, in general, have different charge-transfer rates, and ensemble measurements will result in a signal that is a weighted average of the distribution of these rates.[6] For quasi-spherical nanoparticles, the charge-transfer rate from a state in the particle to a molecule on the surface is largely independent of the position of the molecule, so the distribution of charge-transfer rates is determined primarily by the Poisson distribution of the number of molecules adsorbed on each nanocrystal; ensemble kinetics can thus be modeled to extract charge-transfer rates.[7,8] On the other hand, this assumption is no longer expected to hold for anisotropic nanocrystals, such as the semiconductor nanorods that have shown promising photocatalytic properties.[9−12] This is especially true for nanorod heterostructures composed of more than one semiconductor, which can provide internal separation of the electron and hole and thus improve the

Received: July 23, 2021
Published: September 16, 2021

https://doi.org/10.1021/acs.jpcc.1c06581
J. Phys. Chem. C 2021, 125, 21246−21253

efficiency of charge transfer and extraction.[13] For these heterostructures, such as CdSe/CdS core/shell nanorods,[14−16] the electron wave function may be localized in a particular part of the nanorod,[17,18] so that electron transfer rates to adsorbed molecules will depend strongly on the position of the molecule at the surface of nanorod. While ensemble measurements give information about the average charge-transfer kinetics in such structures, they cannot provide insight into the correlation between the charge-transfer dynamics and the arrangement of the hybrid nanostructure.

Ultimately, this insight can be obtained only be measuring the full distribution of charge-transfer rates, which requires making measurements on individual nanoparticles. Proof-of-principle experiments have demonstrated the feasibility of measuring charge transfer at the level of single nanocrystals.[19−22] Measurements on single quasi-spherical nanocrystals have resolved transfer rates at the single-molecule level,[23] showing that electrons transfer independently from confined states in the nanocrystal to each molecule on the surface (so that the total transfer rate for N adsorbed molecules is simply N times the transfer rate for a single adsorbed molecule) and also showing that the transfer rate from confined states to molecules is independent of the location of the molecule on the nanocrystal surface (since all surface sites are nominally identical for these quasi-spherical particles). These measurements thus validate the assumptions made in the analysis of ensemble data.

On the other hand, the assumption that all surface sites are equivalent is not expected to hold for anisotropic nanocrystals such as nanorods. Single-particle measurements have resolved the distribution of energy-transfer rates from CdSe/CdS core/shell nanorods to acceptor molecules,[24] but there have so far been no measurements of the distributions of charge-transfer rates from anisotropic nanocrystals to molecules.

Here, we applied to CdSe/CdS core/shell nanorods the techniques we previously developed to measure charge-transfer rates from individual CdSe/CdS core/shell quantum dots to single methyl viologen molecules deposited on their surfaces.[23] By comparing the experimental results to the predictions of a tight-binding model, we found that the charge-transfer rate distribution is consistent with the electron transferring to the molecule from the second-lowest energy state in the conduction band of the nanorod (i.e., at higher energy than the conduction-band edge). This "hot-electron" extraction implies a potential route to higher energy efficiency for photocatalytic applications involving these nanorods. The results also demonstrate the application of single-particle charge-transfer measurements to probe the spatial distribution of electron states in semiconductor nanostructures.

METHODS

Materials. Trioctylphosphine (TOP), trioctylphosphine oxide (TOPO), hexadecylamine (HDA), hexylphosphonic acid (HPA), octadecylphosphonic acid (ODPA), toluene, methanol, selenium, and sulfur were all purchased from Sigma-Aldrich and were at least of ACS purity.

Synthesis of CdSe/CdS Core/Shell Nanorods. The 3.1 nm CdSe seeds were prepared by mixing 3.0 g of TOPO, 0.28 g of ODPA, and 0.06 g of CdO. The mixture was kept at 150 °C for 1.5 h. It was then heated to 300 °C, and 1.5 g of TOP was injected. Then, a mixture of 0.36 g of TOP and 0.06 g of Se was injected at 380 °C. The reaction mixture was kept at 380 °C for 3 min. Synthesized CdSe nanocrystals were isolated and purified from unreacted species by using a solvent/nonsolvent deposition technique, with methanol as the nonsolvent and toluene as the solvent and with the process repeated three times. Finally, the CdSe nanocrystals were dissolved in TOP to a concentration of 400 μM.

CdSe/CdS NRs were prepared following previously reported methods.[15,16,25] 3.0 g of TOPO, 0.3 g of ODPA, 0.08 g of HPA, and 0.086 g of CdO were mixed and heated under a N_2 atmosphere up to 150 °C. The solution was then dried by applying vacuum for 1.5 h at 150 °C. Next, the reaction flask containing the mixture was heated to 350 °C under N_2, and 1.5 g of TOP was injected. After the temperature stabilized at 350 °C, a mixture of 0.12 g of S, 1.5 g of TOP, and 200 μL of the CdSe seed solution was injected into the reaction flask. After 6 min, the heating source was removed, and the reaction mixture was allowed to cool. Synthesized CdSe/CdS nanorods were isolated and purified from unreacted species by using a solvent/nonsolvent deposition technique using methanol as the nonsolvent and toluene as the solvent, with the process repeated twice. Finally, the nanorods were dissolved in toluene to $\sim 3 \times 10^{-4}$ mol %.

Preparation of Single Nanorod−Viologen Assemblies. The as-synthesized nanorod sample was diluted in toluene by a factor of 100. Approximately 0.5 mg of methyl viologen powder was added to 0.5 mL of this diluted solution, and the mixture was sonicated for 1 min. This procedure was previously found to result in at most one viologen molecule adsorbed onto each nanoparticle,[23] which we verified by measuring the time-resolved fluorescence of the ensemble of functionalized nanorods. After sonication, the sample was diluted in chloroform by a further factor of 200−500, and this diluted solution was sonicated again for 1 min. We deposited 2.5 μL of this final solution on a cleaned glass coverslip, and the solvent was allowed to evaporate.

Single-Particle Time-Resolved Fluorescence Measurements. Measurements were performed on a home-built single-particle microscope (Figure 1).[23] The nanorod−viologen assemblies on the glass coverslip were illuminated through a 100× oil-immersion objective with ~100 ps pulses at a

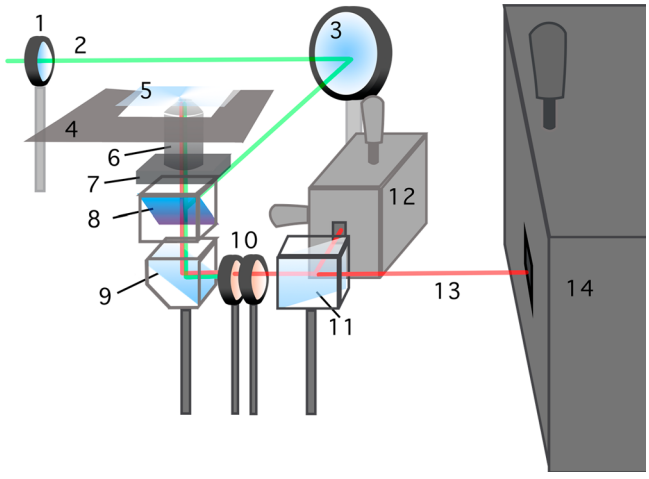

Figure 1. Schematic diagram of the apparatus used for single-particle time-resolved photoluminescence spectroscopy: (1) collimating/focusing lens; (2) incident pulsed laser beam; (3) mirror; (4) sample translation stage; (5) sample; (6) microscope objective; (7) focusing stage; (8) dichroic beamsplitter; (9) mirror; (10) long-pass filters; (11) removable mirror; (12) single-photon detector; (13) output photoluminescence beam; (14) spectrometer.

https://doi.org/10.1021/acs.jpcc.1c06581
J. Phys. Chem. C 2021, 125, 21246−21253

wavelength of 510 nm from a pulsed laser diode (PicoQuant LDH-D-C-510), with an average power of 3.0 mW and a repetition rate of 125 kHz. Fluorescence from individual nanocrystals was collected through the same objective and isolated from reflected laser light with a dichroic filter and two long-pass filters. The emitted light was directed either toward a grating spectrometer (Princeton Instruments Spectra Pro 500i) with a CCD detector (Princeton Instruments Pixis 400) for measurement of fluorescence spectra or toward a single-photon detector (PicoQuant MPD) for measurement of time-dependent fluorescence decay. The time-dependent fluorescence was measured by using the time-correlated single-photon counting technique (PicoQuant PicoHarp 300).

Electronic Structure Calculations. Confined conduction-band states in CdSe/CdS core/shell nanorods were modeled by using the method in ref 18. We employed an sp^3d^5 empirical tight-binding theory, which provides an atomistic theory with an unambiguous modeling of the effects of nanocrystal size, shape, and variations in composition on the monolayer scale. A nine-state atomic-like basis set (s; x; y; z; xy; yz; xz; $x^2 - y^2$; $3z^2 - r^2$) was used to describe each atom in the structure, and interactions were restricted to nearest neighbors only. The inclusion of d orbitals in the minimal basis set is necessary to provide a good description of the bulk-band dispersion at high symmetry points at the edge of the Brillouin zone.[26] This is important in small structures, where mixing of states away from the center of the Brillouin zone is needed to describe strongly confined states. Spin−orbit interactions were described by including only the contributions from the p states; the much smaller splittings of excited d states were neglected.

We assume that the electronic states of a nanorod capped with a single viologen molecule can be modeled by the electron states of a fully passivated nanorod. To mimic the effects of surface passivation by ligands and to eliminate spurious surface states lying inside the gap, we shifted the energies of the sp^3 dangling-bond orbitals on the surface atoms well above the conduction band edge.[27−30] Dangling bonds due to d states do not contribute to the gap states.

Tight-binding parameters taken from ref 31 were changed slightly to better reproduce the bulk bandgaps,[28] and the CdSe/CdS band offsets were obtained from ref 32. The cores and shells were modeled as cylindrical nanorods with hemispherical ends, with the core center located one-half of the distance between the nanorod center and the end of the straight section of the nanorod. We verified using additional calculations that the results are qualitatively unchanged by variations in the position of the core within the shell.

We start each calculation with the atoms in the core−shell structure initially located on the regular lattice of the uniform core material. Such a uniform system exhibits enormous strain because the atoms in the shell are far from their bulk positions. We minimized the strain energy by relaxing the lattice using the valence-force-field method.[27,33,34] In this method, the atoms in the core and shell are allowed to move in any direction to achieve strain relaxation at the interfaces. Minimization of the strain energy was performed by using a combination of steepest-descent and conjugate-gradient techniques. The relaxed atomic positions produce local changes of the bulk tight-binding matrix elements between neighboring atoms (off-site tight-binding parameters V_{kl}). The effects of the relaxed bond angles and atomic positions on the tight-binding matrix elements were calculated by using the Slater−Koster formulas.[35] Power-law scaling was used for the changed bond lengths: $V_{kl} = V_{kl}^0(d_{ij}^0/d_{ij})^\kappa$, where d_{ij} is the bond length between the nearest neighbors i and j and the superscript 0 refers to the unstrained values. A single exponent was sufficient because, in the sp^3d^5 parametrization proposed by Sarma,[31] the hopping parameters obey the universal Harrison scaling law $\kappa = 2$, ensuring transferability to the nanocrystals. We have considered in previous work[18] other larger values of κ and found that the results did not change qualitatively. Once the nanocrystal structure was defined, we found the single-particle electron states by diagonalizing the tight-binding Hamiltonian using an iterative solver.

RESULTS AND DISCUSSION

Figure 2a shows a transmission electron microscope image of CdSe/CdS core/shell nanorods with 3.1 nm cores. The nanorods had uniform cylindrical shapes and rounded end-caps, with average length of 28 nm and average diameter of 4.0 nm. As previously observed for similar nanocrystals,[14−18] absorption in the nanorod ensemble is dominated by the CdS band edge due to the much larger volume of CdS than CdSe in the nanorods. Carriers excited into the CdS shell rapidly relax to states near the CdSe band edge, and fluorescence occurs from these lower-energy states (see Figure 2b). Time-resolved fluorescence measurements on the nanorod ensemble show changes in the emission dynamics when viologen molecules are adsorbed on the nanorod surfaces (see Figure 2c). It is difficult, however, to obtain quantitative information about charge-transfer rates from these ensemble measurements because of heterogeneity in charge-transfer rates among all the nanorods in the ensemble.

As shown in Figure 3a, fluorescence spectra measured from individual nanorods were significantly narrower than the ensemble fluorescence spectrum due to the removal of inhomogeneous broadening. The narrow line width was used to distinguish single nanorods from clusters, with time-resolved fluorescence measurements being collected only if the measured fluorescence line width was narrower than 16 nm.

For the isolated nanorods, our goal is to determine the distribution of charge-transfer rates, γ_{ct}, from quantum-confined conduction-band states in the nanorods to single viologen molecules on the surface. The measurable physical quantity, however, is the total decay rate of a photoexcited exciton in a nanorod, $\gamma_{tot} = \gamma_{rad} + \gamma_{ct}$, which includes both the rate of charge transfer and the rate of radiative recombination of the confined conduction-band electron with a confined valence-band hole, γ_{rad}. Determination of the distribution of γ_{ct} thus requires comparison between the distributions of γ_{tot} for the viologen-functionalized nanorods and the control sample without viologen molecules (for which $\gamma_{ct} = 0$).

The time-averaged fluorescence decay from a single nanorod includes both radiative and nonradiative recombination processes. To isolate the radiative recombination rates, we measured the fluorescence intensity from each nanorod as a function of time. These time traces typically showed strong intermittency, or blinking,[36] as illustrated in Figure 3b. This blinking corresponds to fluctuations in nonradiative recombination rate, with the nonradiative rate close to zero when the fluorescence intensity is highest (i.e., when the nanorod is in its "bright" state).[37] We were therefore able to eliminate the effects of the nonradiative recombination by applying an intensity threshold and discarding all the photons collected when the intensity is below this threshold (see Figure 3b). A histogram of delay times between detection of the "bright-state" photons and the corresponding excitation laser pulse thus produced a time-

https://doi.org/10.1021/acs.jpcc.1c06581
J. Phys. Chem. C 2021, 125, 21246−21253

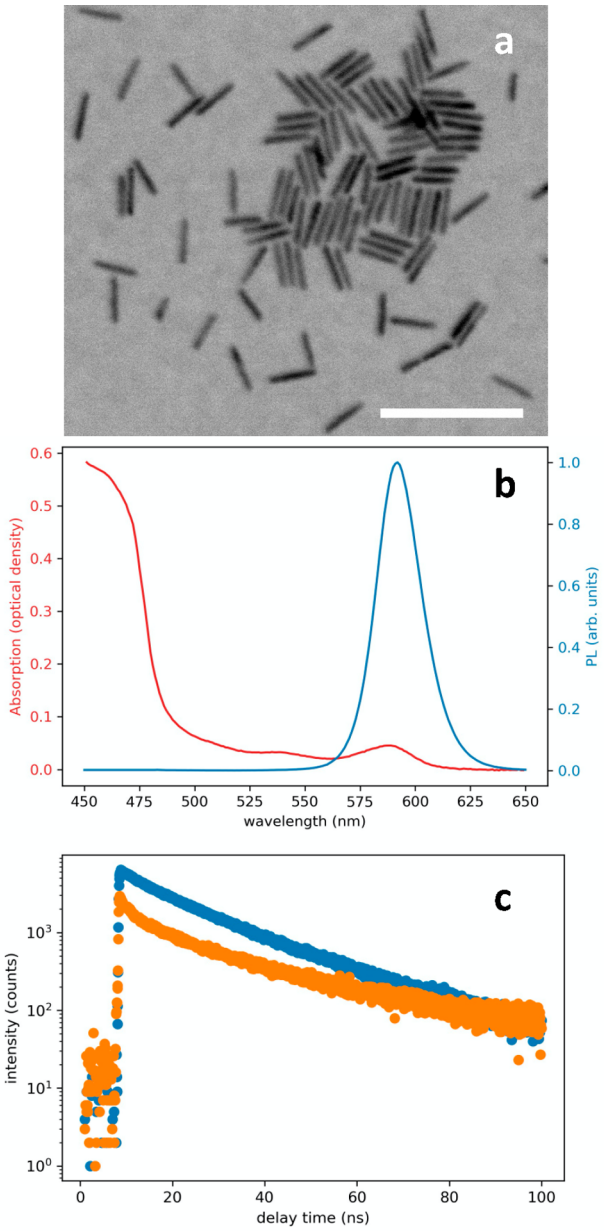

Figure 2. (a) Transmission electron microscope image of CdSe/CdS core/shell nanorods. The scale bar is 100 nm. (b) Absorption (red) and photoluminescence (PL, blue) spectra for an ensemble of as-synthesized CdSe/CdS core/shell nanorods. (c) Time-resolved fluorescence decay curves for an ensemble of CdSe/CdS core/shell nanorods before (blue) and after (orange) being functionalized with viologen molecules.

resolved photoluminescence decay curve with a single-exponential decay corresponding to γ_{tot} (Figure 3c).[23]

Figure 3d shows a histogram of the decay rates, γ_{tot}, measured for the viologen-functionalized sample and for the unfunctionalized control sample. For the control sample, the distribution of decay rates corresponds to the distribution of radiative recombination rates in the nanorod sample and is well represented by a normal distribution with an average decay rate of 0.085 ns^{-1} and a standard deviation of 0.017 ns^{-1}. The relatively narrow distribution of decay rates for this as-synthesized sample indicates a high degree of uniformity within the nanorod ensemble, not only in terms of their structure but also in terms of their electronic properties.

By comparison, the distribution of decay rates for the sample with adsorbed viologen showed a shoulder and a long tail toward higher rates (Figure 3d). Because the shift between this histogram and the control histogram corresponds to the distribution of γ_{ct} in the sample, the data indicate that there were several nanorods with moderate charge-transfer rates and a small number of nanorods with much larger charge-transfer rates.

This is in contrast to results previously obtained on quasi-spherical CdSe/CdS core/shell nanocrystals;[23] if at most a single molecule were adsorbed on the quasi-spherical quantum dots, the effect would simply be to reproduce the Gaussian histogram of decay rates, shifted by a constant value of γ_{ct}. The broad distribution for the viologen-functionalized nanorod sample thus reflects a broad distribution of charge-transfer rates from the nanorods to adsorbed viologen molecules. Because the sample was prepared such that there is at most one molecule on the surface of each nanorod, the broad distribution of charge-transfer rates is most likely due to variation in the position of the adsorbed molecule on the surface of the nanorod.

In Marcus electron-transfer theory,[38] the transfer rate is proportional to the matrix element between the confined electron state of the donor nanocrystal and the molecular orbital in the acceptor molecule. Assuming that the molecules are small enough compared to the nanorods that they can be treated as point acceptors, the charge-transfer rate is proportional to the probability (i.e., the charge density) of the confined electron wave function at the surface site on the nanorod where the viologen molecule is attached, P_s. If the molecules are equally likely to be adsorbed at any position on the nanorod, and if the capture rate onto the molecule from the surface site, γ_c, is the same for all surface sites, then the distribution of γ_{ct} is given by the distribution of P_s.

We therefore modeled the distribution of decay rates by first calculating the confined electron states in the nanorod by using the tight-binding model and then calculating P_s from the electron wave function at each surface site. Figure 4a shows P_s as a function of the position, Z, along the axis of the nanorod, where $Z = 0$ corresponds to the center of the CdSe core. Results are shown for the lowest-energy state in the conduction band, E_1, and for the second-lowest-energy state, E_2, located 140 meV above E_1 (see the inset of Figure 4a). Also shown for comparison in Figure 4a are the electron probabilities for sites along the axis of the nanorod. The dispersion of probabilities for the surface sites reflects the four different atoms in the unit cell that can be located at the nanorod surface (two for Cd and two for S). Electrons in E_1 can be seen to be localized primarily in the CdSe core (around $Z = 0$, where electrons in E_2 are delocalized throughout the CdS shell (primarily at $Z < 0$, to ensure orthogonality with E_1); see Figure 4a.

The distribution of P_s was simply obtained by taking a histogram of the results in Figure 4a; Figure 4b shows the results for the two lowest-energy electron states. Both distributions have a large maximum near zero, corresponding to the large fraction of surface sites with low electron probability. The distribution for E_1 is almost entirely localized around low probabilities, whereas the distribution for E_2 has a long tail extending out to larger values of P_s; this reflects the greater delocalization of E_2 as compared to E_1.

From this distribution of P_s, we obtained the distribution of decay rates as $\gamma_{tot} = \gamma_c P_s + \gamma_{rad}$. The radiative decay rate, γ_{rad}, is obtained from the control sample, and γ_c is treated as an adjustable parameter for comparison to experiment. In this

https://doi.org/10.1021/acs.jpcc.1c06581
J. Phys. Chem. C 2021, 125, 21246−21253

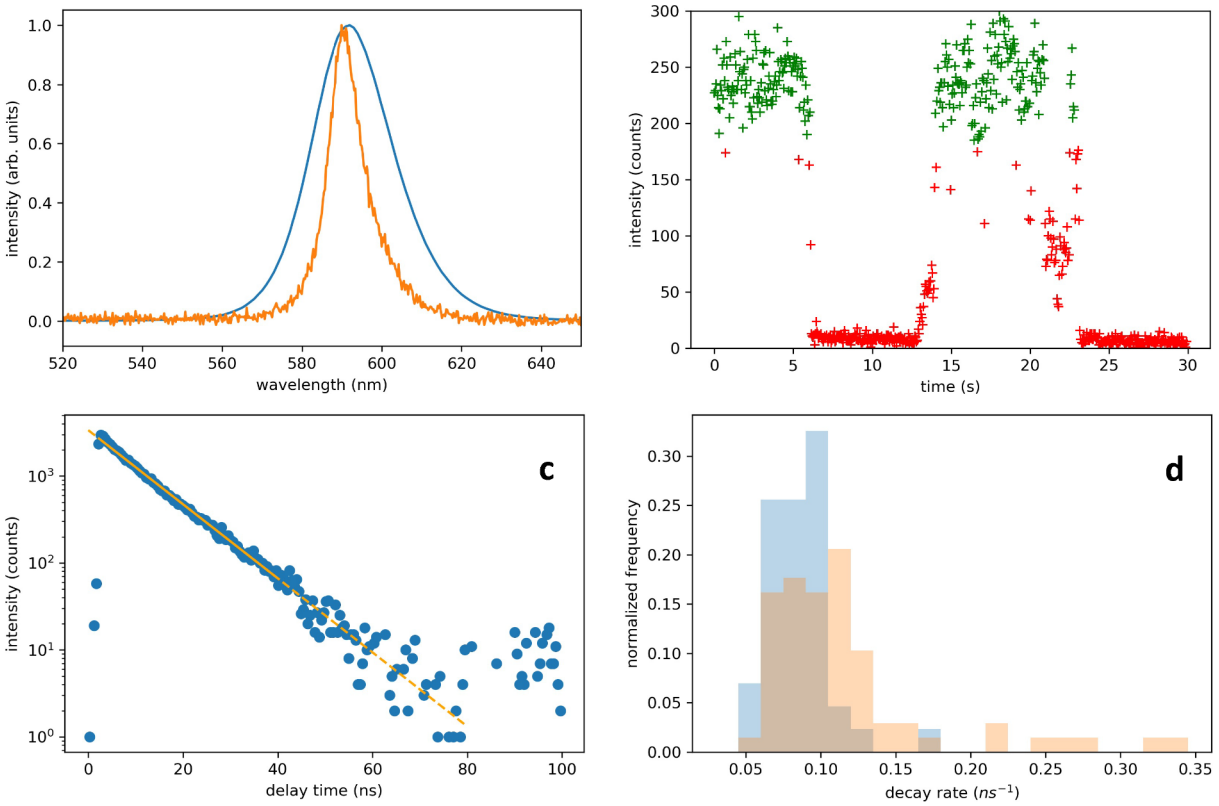

Figure 3. (a) Photoluminescence from an ensemble of CdSe/CdS core/shell nanorods (blue) and from a single nanorod (orange). (b) Fluorescence intensity as a function of time from a single CdSe/CdS core/shell nanorod. A threshold intensity was applied to distinguish "bright" and "dark" states; green points are above this threshold, and red points are below. (c) Time-resolved fluorescence decay curve for a single CdSe/CdS core/shell nanorod calculated by using only photons emitted when the fluorescence intensity is above the "bright-state" threshold. Background counts are subtracted by measuring the average count rate before arrival of the excitation laser pulse. Points are experimental values, and the line is a single-exponential fit; the solid line corresponds to the range of delay times used for the fit, and the dashed line shows the extrapolation of this fit. The slope of this line gives the total decay rate, γ_{tot}, equal to the sum of the radiative recombination rate and the charge-transfer rate. (d) Histogram of decay rates, γ_{tot}, from single CdSe/CdS core/shell nanorods, comparing a sample that has at most one viologen molecule adsorbed on each nanorod (red) to a control sample with no viologen (blue).

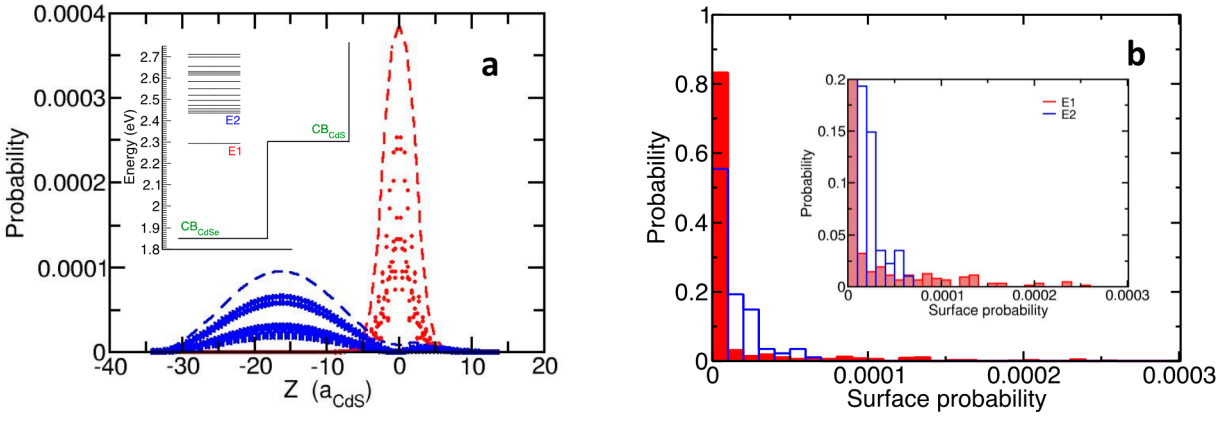

Figure 4. (a) Calculated probability density, P_s, for the two lowest-energy states, E_1 (red) and E_2 (blue), as a function of axial position, Z, along a CdSe/CdS core−shell nanorod. The core diameter is 3.1 nm, the nanorod diameter is 4.0 nm, and the nanorod length is 28 nm, including hemispherical caps on each end of the nanorod. $Z = 0$ corresponds to the center of the core, which is located halfway between the center of the nanorod and the beginning of one of the hemispherical caps. Results are shown for atomic sites at the surface of the nanorod (points) and atomic sites along the axis of the nanorod (dashed lines). The inset shows the energies of electron states in the conduction band, with E_1 and E_2 labeled. (b) Probability distribution of P_s for E_1 (red) and E_2 (blue). The inset shows the same data with a different vertical scale.

model, we assume that any differences in charge-transfer rates are due only to differences in the position of the viologen molecules on the nanorod surfaces and not due to differences among the nanorods; this assumption is justified by the high degree of uniformity for this nanorod structure, in terms of both their structure and their electron dynamics.

Results are shown in Figure 5 for E_1 and E_2 and for representative values of γ_c. The differences between the

https://doi.org/10.1021/acs.jpcc.1c06581
J. Phys. Chem. C 2021, 125, 21246−21253

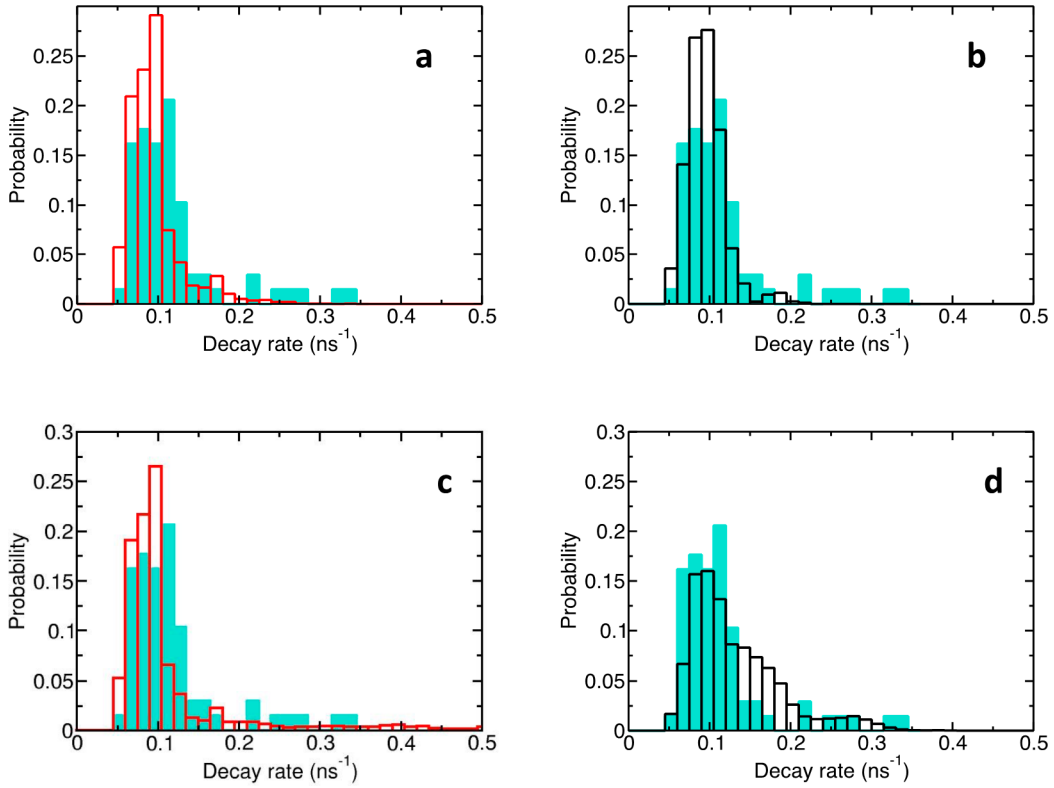

Figure 5. Experimental (filled bars) and theoretical (hollow bars) probability distributions for the decay rate, γ_{tot}, of electrons in quantum-confined conduction-band states in CdSe/CdS core/shell nanorods with single viologen acceptor molecules on their surfaces. Theoretical results are based on $\gamma_{tot} = \gamma_c P_s + \gamma_{rad}$, where P_s is the calculated probability of the electron being at the surface site where the molecule is located, γ_{rad} is the radiative decay rate (determined from measurements on a control sample without molecules), and γ_c is the assumed capture rate from the surface site to the molecule. Model results are shown for (a) the lowest energy state, E_1, and $\gamma_c = 0.65$ ps^{-1}; (b) the second-lowest energy state, E_2, and $\gamma_c = 0.65$ ps^{-1}; (c) E_1 and $\gamma_c = 3.47$ ps^{-1}; and (d) E_2 and $\gamma_c = 3.47$ ps^{-1}.

calculated histograms for the different electron states reflect the differences in the distribution of surface-state probabilities (see Figure 4b). The calculated histograms for E_1 (Figure 5a,c) do not provide a good qualitative representation of the experimental histogram regardless of the assumed value of γ_c. For $\gamma_c = 0.65$ ps^{-1}, the tail of high decay rates is much smaller for the theoretical calculation than for the experimental data; for $\gamma_c = 3.47$ ps^{-1}, the tail is somewhat larger but extends to much higher decay rates than the experimental data. Moreover, in both cases, the theoretical data fail to reproduce the shoulder of slightly higher decay rates next to the main peak in the histogram. The calculated histogram for E_2 and $\gamma_c = 0.65$ ps^{-1} (Figure 5b) is also in poor qualitative agreement with the experiment, failing to reproduce the tail of high decay rates. In contrast, the calculated histogram for E_2 and $\gamma_c = 3.47$ ps^{-1} (Figure 5d) reproduces qualitatively the main features of the experimental histogram, namely, the shoulder around the main peak and the tail of high decay rates. The theoretical shoulder is somewhat higher than in the experimental data; nonetheless, the qualitative agreement between theory and experiment seems to be better for E_2 than for E_1. This better agreement ultimately stems from the greater degree of delocalization in E_2.

The results thus suggest that electron transfer occurs from E_2 to the viologen molecules. In other words, the rate of relaxation from E_2 to E_1 appears to be slow compared to the rate of electron transfer from E_2 to an adsorbed viologen molecule, so that relaxation does not compete with charge transfer. This is somewhat surprising because intraband relaxation in semiconductor nanocrystals generally occurs on subnanosecond time scales,[39] while the fastest measured decay rates in the current samples correspond to electron-transfer times of ~4 ns. However, our previous transient-absorption measurements on similar CdSe/CdS core/shell nanorods have been consistent with slow relaxation from E_2 to E_1, slower in fact than radiative recombination with holes in the valence band.[18] Ensemble[40] and single-particle[41] fluorescence measurements have also indicated an inhibited relaxation in CdSe/CdS core/shell tetrapod nanocrystals. Our current results provide additional support for a bottleneck for intraband relaxation between electron states in CdSe/CdS nanocrystal heterostructures.

CONCLUSIONS

We measured the distribution of decay rates of excitons in individual CdSe/CdS core/shell nanorods with single electron-accepting molecules on their surfaces. By comparing this distribution to the equivalent distribution for nanorods with no adsorbed molecules, we inferred the distribution of electron transfer-rates from confined electron states in the nanorods to states in the single molecules. Tight-binding models of transfer-rate distributions are consistent with experimental results only if we assume that electron transfer occurs from the second-lowest electron energy state in the conduction band, E_2, rather than the lowest energy state, E_1. The results thus suggest that electron transfer from E_2 is faster than intraband relaxation to E_1.

Transferring an electron out of a higher-energy state in a nanocrystal means that the charge-separated state can have higher energy than it would if the charge were extracted after it thermalizes to the lowest-energy state in the conduction

https://doi.org/10.1021/acs.jpcc.1c06581
J. Phys. Chem. C 2021, 125, 21246−21253

band.[42,43] This "hot-electron" transfer thus has the potential to enable higher energy efficiency for solar energy conversion using these materials.[44] Although the energy separation between E_1 and E_2 is relatively modest, it may be possible to engineer nanocrystal heterostructures with different geometries or out of different materials to increase the energy-level separation and permit the efficient extraction of higher-energy electrons. If the states in the accepting molecule (or other accepting nanostructure) are close in energy to the "hot-electron" state in the nanocrystal, then a larger fraction of the energy in incident high-energy photons can be used; moreover, it may be possible to drive photocatalytic reactions that are otherwise energetically inaccessible.

Even though reasonable agreement is obtained between the experimental and theoretical decay-rate distributions when assuming electron transfer from E_2, there are still differences between the two. These differences may be due to the approximations made in the theoretical model. Perhaps most significantly, the electronic structure calculations do not consider Coulombic interactions and correlation effects between the electron and hole in the nanorods. Some previous studies have suggested that excitons are formed between conduction-band electrons and holes localized in trap states on the nanorod surface;[45,46] if this occurs, it will significantly impact electron-transfer rates. We note, however, that the experimental results indicate electron delocalization rather than localization. In addition, the highly uniform recombination dynamics for the as-synthesized nanorods implies that surface traps are not playing a significant role in the carrier dynamics for this nanorod sample. This degree of uniformity is specific to the nanorod sample studied and the growth process used to synthesize the sample; for longer nanorods, in particular, trapping and electron localization are likely to be more significant.

The main reason for the difference between the theoretical and experimental histograms is thus likely to be statistical noise due to the limited number of nanorods that were measured. More quantitative comparison to theory will require measuring the decay rates for a significantly larger number of particles, which may be possible by using single-photon-detector arrays[47] or other wide-field fluorescence-lifetime imaging techniques.[48] In this way, the method of measuring charge-transfer-rate distributions could become a broadly applicable tool to probe the spatial properties of confined carrier states in nanocrystals, complementing sophisticated techniques such as scanning tunneling spectroscopy.[49]

AUTHOR INFORMATION

Corresponding Author

Matthew Pelton − *Department of Physics, University of Maryland, Baltimore County (UMBC), Baltimore, Maryland 20912, United States;* orcid.org/0000-0002-6370-8765; Email: mpelton@umbc.edu

Authors

Rachel M. Morin − *Department of Physics, University of Maryland, Baltimore County (UMBC), Baltimore, Maryland 20912, United States*

Garnett W. Bryant − *Nanoscale Device Characterization Division and Joint Quantum Institute, National Institute of Standards and Technology, Gaithersburg, Maryland 20899, United States*

Elena V. Shevchenko − *Center for Nanoscale Materials, Argonne National Laboratory, Argonne, Illinois 60439, United States;* orcid.org/0000-0002-5565-2060

Yuchen Sha − *Center for Nanoscale Materials, Argonne National Laboratory, Argonne, Illinois 60439, United States; Institute of Advanced Studies (IAS), College of Chemistry and Molecular Science, Wuhan University, Wuhan 430072 Hubei, China*

Complete contact information is available at: https://pubs.acs.org/10.1021/acs.jpcc.1c06581

Notes

The authors declare no competing financial interest.

ACKNOWLEDGMENTS

We thank Haixu Leng and Vijin Kizhake Veetil for experimental assistance. R.M.M. acknowledges support from UMBC through the URA program. Work at the Center for Nanoscale Materials was supported by the U.S. Department of Energy, Office of Science, Office of Basic Energy Sciences, under Contract DE-AC0206CH-11357. Product names are mentioned to provide an accurate record of what was done. Reference of product names does not constitute validation or endorsement.

REFERENCES

(1) Tachibana, Y.; Vayssieres, L.; Durrant, J. R. Artificial Photosynthesis for Solar Water-Splitting. *Nat. Photonics* **2012**, *6*, 511−518.

(2) Kamat, P. V. Meeting the Clean Energy Demand: Nanostructure Architectures for Solar Energy Conversion. *J. Phys. Chem. C* **2007**, *111*, 2834−2860.

(3) Tong, H.; Ouyang, S.; Bi, Y.; Umezawa, N.; Oshikiri, M.; Ye, J. Nano-photocatalytic Materials: Possibilities and Challenges. *Adv. Mater.* **2012**, *24*, 229−251.

(4) Low, J.; Yu, J.; Jaroniec, M.; Wageh, S.; Al-Ghamdi, A. A. Heterojunction Photocatalysis. *Adv. Mater.* **2017**, *29*, 1601694.

(5) Irgen-Gioro, S.; Yang, M.; Padgaonkar, S.; Chang, W. J.; Zhang, Z.; Nagasing, B.; Jiang, Y.; Weiss, E. A. Charge and Energy Transfer in the Context of Colloidal Nanocrystals. *Chem. Phys. Rev.* **2020**, *1*, 011305.

(6) Knowles, K. E.; Peterson, M. D.; McPhail, M. R.; Weiss, E. A. Exciton Dissociation within Quantum Dot-Organic Complexes: Mechanisms, Use as a Probe of Interfacial Structure, and Applications. *J. Phys. Chem. C* **2013**, *117*, 10229−10243.

(7) Sadhu, S.; Tachiya, M.; Patra, A. A. Stochastic Model for Energy Transfer from CdS Quantum Dots/Rods (Donors) to Nile Red Dye (Acceptors). *J. Phys. Chem. C* **2009**, *113*, 19488−19492.

(8) Morris-Cohen, A. J.; Frederick, M. T.; Cass, L. C.; Weiss, E. A. Simultaneous Determination of the Adsorption Constant and the Photoinduced Electron Transfer Rate for a CdS Quantum Dot-Viologen Complex. *J. Am. Chem. Soc.* **2011**, *133*, 10146−10154.

(9) Amirav, L.; Alivisatos, A. P. Photocatalytic Hydrogen Production with Tunable Nanorod Heterostructures. *J. Phys. Chem. Lett.* **2010**, *1*, 1051−1054.

(10) Brown, K. A.; Wilker, M. B.; Boehm, M.; Dukovic, H.; King, P. W. Characterization of Photochemical Processes for H_2 Production by CdS Nanorod-[FeFe] Hydrogenase Complexes. *J. Am. Chem. Soc.* **2012**, *134*, 5627−5636.

(11) Wu, K.; Du, Y.; Tang, H.; Chen, Z.; Lian, T. Efficient Exctraction of Trapped Holes from Colloidal CdS Nanorods. *J. Am. Chem. Soc.* **2015**, *137*, 10224−10230.

(12) Wolff, C. M.; Frischmann, P. D.; Schulze, M.; Bohn, B. J.; Wein, R.; Livadas, R.; Carlson, M. T.; Jäckel, F.; Feldmann, J.; Würthner, F.; Stolarczyk, J. K. All-In-One Visible-Light-Driven Water Splitting by Combining Nanoparticulate and Molecular Co-Catalysts on CdS Nanorods. *Nat. Energy* **2018**, *3*, 862−869.

(13) Zhu, H.; Lian, T. Wavefunction Engineering in Quantum Confined Semiconductor Nanoheterostructures for Efficient Charge

Separation and Solar Energy Conversion. *Energy Environ. Sci.* **2012**, *5*, 9406−9418.
(14) Talapin, D. V.; Koeppe, R.; Gotzinger, S.; Kornowski, A.; Lupton, J. M.; Rogach, A. L.; Benson, O.; Feldmann, J.; Weller, H. Highly Emissive Colloidal CdSe/CdS Heterostructures of Mixed Dimensionality. *Nano Lett.* **2003**, *3*, 1677−1681.
(15) Talapin, D. V.; Nelson, J. H.; Shevchenko, E. V.; Aloni, S.; Sadtler, B.; Alivisatos, A. P. Seeded Growth of Highly Luminescent CdSe/CdS Nanoheterostructures with Rod and Tetrapod Morphologies. *Nano Lett.* **2007**, *7*, 2951−2959.
(16) Carbone, L.; Nobile, C.; De Giorgi, M.; Sala, F. D.; Morello, G.; Pompa, P.; Hytch, M.; Snoeck, E.; Fiore, A.; Franchini, I. R.; et al. Synthesis and Micrometer-Scale Assembly of Colloidal CdSe/CdS Nanorods Prepared by a Seeded Growth Approach. *Nano Lett.* **2007**, *7*, 2942−2950.
(17) Muller, J.; Lupton, J. M.; Lagoudakis, P. G.; Schindler, F.; Koeppe, R.; Rogach, A. L.; Feldmann, J.; Talapin, D. V.; Weller, H. Wave Function Engineering in Elongated Semiconductor Nanocrystals with Heterogeneous Carrier Confinement. *Nano Lett.* **2005**, *5*, 2044−2049.
(18) She, C.; Bryant, G. W.; Demortière, A.; Shevchenko, E. V.; Pelton, M. Controlling the Spatial Location of Photoexcited Electrons in CdSe/CdS Core/Shell Nanorods. *Phys. Rev. B: Condens. Matter Mater. Phys.* **2013**, *87*, 155427.
(19) Issac, A.; Jin, S.; Lian, T. Intermittent Electron Transfer Activity from Single CdSe/ZnS Quantum Dots. *J. Am. Chem. Soc.* **2008**, *130*, 11280−11281.
(20) Cui, S.-C.; Tachikawa, T.; Fujitsuka, M.; Majima, T. Interfacial Electron Transfer Dynamics in a Single CdTe Quantum Dot-Pyromellitimide Conjugate. *J. Phys. Chem. C* **2008**, *112*, 19625−19634.
(21) Song, N.; Zhu, H.; Jin, S.; Zhan, W.; Lian, T. Poisson-Distributed Electron-Transfer Dynamics from Single Quantum Dots to C_{60} Molecules. *ACS Nano* **2011**, *5*, 613−621.
(22) Chen, J.-S.; Li, M.; Cotlet, M. Nanoscale Photoinduced Charge Transfer with Individual Quantum Dots: Tunability through Synthesis, Interface Design, and Interaction with Charge Traps. *ACS Omega* **2019**, *4*, 9102−9112.
(23) Leng, H.; Loy, J.; Amin, V.; Weiss, E. A.; Pelton, M. Electron Transfer from Single Semiconductor Nanocrystals to Individual Acceptor Molecules. *ACS Energy Lett.* **2016**, *1*, 9−15.
(24) Hadar, I.; Halivni, S.; Even-Dar, N.; Faust, A.; Banin, U. Dimensionality Effects on Fluorescence Resonance Energy Transfer between Single Semiconductor Nanocrystals and Multiple Dye Acceptors. *J. Phys. Chem. C* **2015**, *119*, 3849−3856.
(25) Sha, Y.; Lin, X.-M.; Niklas, J.; Poluektov, O. G.; Diroll, B. T.; Lin, Y.; Wen, J.; Hood, Z. D.; Lei, A.; Shevchenko, E. V. Insights into the Extraction of Photogenerated Holes from CdSe/CdS Nanorods for Oxidative Organic Catalysis. *J. Mater. Chem. A* **2021**, *9*, 12690−12699.
(26) Jancu, J. M.; Scholz, R.; Beltram, F.; Bassani, F. Empirical spds* Tight-Binding Calculation for Cubic Semiconductors: General Method and Material Parameters. *Phys. Rev. B: Condens. Matter Mater. Phys.* **1998**, *57*, 6493−6506.
(27) Diaz, J. G.; Bryant, G. W. Electronic and Optical Fine Structure of GaAs Nanocrystals: The Role of d Orbitals in a Tight-Binding Approach. *Phys. Rev. B: Condens. Matter Mater. Phys.* **2006**, *73*, 075329.
(28) Diaz, J. G.; Zielinski, M.; Jaskolski, W.; Bryant, G. W. Tight-binding Theory of ZnS/CdS Nanoheterostructures: The Role of Strain and d Orbitals. *Phys. Rev. B: Condens. Matter Mater. Phys.* **2006**, *74*, 205309.
(29) Diaz, J. G.; Bryant, G. W.; Jaskolski, W.; Zielinski, M. Theory of InP Nanocrystals under Pressure. *Phys. Rev. B: Condens. Matter Mater. Phys.* **2007**, *75*, 245433.
(30) Bryant, G. W.; Jaskolski, W. Surface Effects on Capped and Uncapped Nanocrystals. *J. Phys. Chem. B* **2005**, *109*, 19650−19656.
(31) Sapra, S.; Shanthi, N.; Sarma, D. D. Realistic Tight-Binding Model for the Electronic Structure of II-VI Semiconductors. *Phys. Rev. B: Condens. Matter Mater. Phys.* **2002**, *66*, 205202.
(32) Wei, S. H.; Zunger, A. Calculated Natural Band Offsets of all II-VI and III-V Semiconductors: Chemical Trends and the Role of Cation d Orbitals. *Appl. Phys. Lett.* **1998**, *72*, 2011−2013.
(33) Saito, T.; Arakawa, Y. Electronic Structure of Piezoelectric $In_{0.2}Ga_{0.8}N$ Quantum Dots in GaN Calculated Using a Tight-Binding Method. *Phys. E* **2002**, *15*, 169−181.
(34) Pryor, S.; Kim, J.; Wang, L. W.; Williamson, A. J.; Zunger, A. Comparison of Two Methods for Describing the Strain Profiles in Quantum Dots. *J. Appl. Phys.* **1998**, *83*, 2548−2554.
(35) Slater, J. C.; Koster, G. F. Simplified LCAO Method for the Periodic Potential Problem. *Phys. Rev.* **1954**, *94*, 1498−1524.
(36) Nirmal, M.; Dabbousi, B. O.; Bawendi, M. G.; Macklin, J.; Trautman, J. K.; Harris, T. D.; Brus, L. E. Fluorescence Intermittency in Single Cadmium Selenide Nanocrystals. *Nature* **1996**, *383*, 802−804.
(37) Fisher, B. R.; Eisler, H. J.; Stott, N. E.; Bawendi, M. G. Emission Intensity Dependence and Single-Exponential Behavior in Single Colloidal Quantum Dot Fluorescence Lifetimes. *J. Phys. Chem. B* **2004**, *108*, 143−148.
(38) Marcus, R. A. On the Theory of Oxidation-Reduction Reactions Involving Electron Transfer. I. *J. Chem. Phys.* **1956**, *24*, 966−978.
(39) Klimov, V. I. Optical Nonlinearities and Ultrafast Carrier Dynamics in Semiconductor Nanocrystals. *J. Phys. Chem. B* **2000**, *104*, 6112−6123.
(40) Choi, C. L.; Li, H.; Olson, A. C. K.; Jain, P. K.; Sivasankar, S.; Alivisatos, A. P. Spatially Indirect Emission in a Luminescent Nanocrystal Molecule. *Nano Lett.* **2011**, *11*, 2358−2362.
(41) Shafran, E.; Borys, N. J.; Huang, J.; Talapin, D. V.; Lupton, J. M. Indirect Exciton Formation due to Inhibited Carrier Thermalization in Single CdSe/CdS Nanocrystals. *J. Phys. Chem. Lett.* **2013**, *4*, 691−697.
(42) Pandey, A.; Guyot-Sionnest, P. Hot Electron Extraction from Colloidal Quantum Dots. *J. Phys. Chem. Lett.* **2010**, *1*, 45−47.
(43) Tisdale, W. A.; Williams, K. J.; Timp, B. A.; Norris, D. J.; Aydil, E. S.; Zhu, X.- Y. Hot-Electron Transfer from Semiconductor Nanocrystals. *Science* **2010**, *328*, 1543−1547.
(44) Nozik, A. J. Quantum Dot Solar Cells. *Phys. E* **2002**, *14*, 115−120.
(45) Wu, K.; Rodriguez-Córdoba, W. E.; Liu, Z.; Zhu, H.; Lian, T. Beyond Band Alignment: Hole Localization Driven Formation of Three Spatially Separated Long-Lived Exciton States in CdSe/CdS Nanorods. *ACS Nano* **2013**, *7*, 7173−7185.
(46) Wu, K.; Hill, L. J.; Chen, G.; McBride, J. R.; Pavlopolous, N. G.; Richey, N. E.; Pyun, J.; Lian, T. Universal Length Dependence of Rod-to-Seed Exciton Localization Efficiency in Type I and Quasi-Type II CdSe@CdS Nanorods. *ACS Nano* **2015**, *9*, 4591−4599.
(47) Bruschini, C.; Homulle, H.; Antolovic, I. M.; Burri, S.; Charbon, E. Single-Photon Avalanche Diode Imagers in Biophotonics: Review and Outlook. *Light: Sci. Appl.* **2019**, *8*, 87.
(48) Hirvonen, L. M.; Suhling, K. Wide-Field TCSPC: Methods and Applications. *Meas. Sci. Technol.* **2017**, *28*, 012003.
(49) Swart, I.; Liljeroth, P.; Vanmaekelbergh, D. Scanning Probe Microscopy and Spectroscopy of Colloidal Semiconductor Nanocrystals and Assembled Structures. *Chem. Rev.* **2016**, *116*, 11181−11219.

https://doi.org/10.1021/acs.jpcc.1c06581
J. Phys. Chem. C 2021, 125, 21246−21253